Polar Climate Simulation of the NCAR CCM3[*,+]

BRUCE P. BRIEGLEB

National Center for Atmospheric Research,[#] Boulder, Colorado

DAVID H. BROMWICH

Polar Meteorology Group, Byrd Polar Research Center, Ohio State University, Columbus, Ohio

(Manuscript received 18 June 1997, in final form 11 November 1997)

ABSTRACT

Present-day Arctic and Antarctic climate of the National Center for Atmospheric Research (NCAR) Community Climate Model version 3 (CCM3) is presented. The CCM3 simulation is from a prescribed and interannually varying sea surface temperature integration from January 1979 through August 1993. Observations from a variety of sources, including the European Centre for Medium-Range Weather Forecasts analyses, rawinsonde, and surface station data, are used for validation of CCM3's polar climate during this period. Overall, CCM3 can simulate many important polar climatic features and in general is an incremental improvement over CCM2.

The 500-hPa polar vortex minima are too deep by 50–100 m and too zonally symmetric. The Arctic sea level pressure maximum is displaced poleward, while the Icelandic region minimum is extended toward Europe, and the Aleutian region minimum is extended toward Asia. The Antarctic circumpolar trough of low sea level pressure is slightly north of the observed position and is 2–3 hPa too low. Antarctic katabatic winds are similar to observations in magnitude and regional variation. The Antarctic surface wind stress is estimated to be 30%–50% too strong in some regions. Polar tropospheric temperatures are 2°–4°C colder than observations, mostly in the summer season. Low-level winter inversions over the Arctic Ocean are only 3°–4°C, rather than the observed 10°C. In the Antarctic midcontinent they are around 25°–30°C (about 5° stronger than observed) and continue to be stronger than observed along the coast. Although water vapor column is uniformly low by 10%–20% compared to analyses in both polar regions, the regional patterns of minima over Greenland and the East Antarctic plateau are well represented. Annual 70° to pole CCM3 values are 5.8 kg m^{-2} for the Arctic and 1.7 kg m^{-2} for the Antarctic. The regional distribution of precipitation minus evaporation compares reasonably with analyses. The annual 70° to pole values are 18.1 cm yr^{-1}, which are close to the most recent observational estimates of 16 to 18 cm yr^{-1} in the Arctic and 18.4 $\pm$ 3.7 cm yr^{-1} in the Antarctic. In both polar regions, summer surface energy budgets are estimated to be low by roughly 20 W m^{-2}.

Suggestions as to causes of simulation deficiencies are 1) polar heat sinks that are too strong; 2) inadequate representation of sea-ice–atmosphere heat exchange, due to lack of fractional coverage of sea ice of variable thickness; 3) effects of low horizontal resolution; and 4) biased extrapolar influence.

1. Introduction

The present issue contains many papers on the National Center for Atmospheric Research (NCAR) climate system model (CSM), a comprehensive global climate model consisting of four components (atmosphere, ocean, land, and sea ice), coupled together by the flux coupler. A critical requirement for the CSM component models is that they adequately simulate present-day climate when forced by observed boundary conditions. The success of the CSM 300-yr coupled integration in preventing large climate drifts is due in part to realistic uncoupled component simulations. An overview of the NCAR CSM is given by Boville and Gent (1998).

Also contained in the present issue are several papers on the simulation of the uncoupled atmospheric component of CSM–NCAR Community Climate Model version 3 (CCM3). In the uncoupled integrations, CCM3 is forced by prescribed monthly sea surface temperatures and sea ice distribution from January 1979 through August 1993, allowing for a comparison of the model simulation with recent observations and analyses. The CCM3 is presented in Kiehl et al. (1998a), while the simulation of the energy budget is discussed in Kiehl et al. (1998b), the dynamical simulation is described in Hurrell et al. (1998), the hydrologic and thermodynamic

structure is considered in Hack et al. (1998), and the land surface simulation is presented in Bonan (1998). These papers deal primarily with the Tropics and midlatitudes, and less with the polar regions. However, with the advent of coupled climate models such as CSM, it is crucial for the polar regions to be adequately simulated as well. The accuracy of the CSM atmospheric and oceanic general circulation depends not only on realistic heat sources (mostly tropical), but also on realistic heat sinks (mostly polar).

Several papers have considered the polar simulations of the two previous versions of CCM (CCM1 and CCM2): Battisti et al. (1992), Tzeng et al. (1993), Bromwich et al. (1994), Tzeng and Bromwich (1994), Tzeng et al. (1994), Bromwich et al. (1995a), and Williamson et al. (1996). These papers show large biases in the CCM1 polar simulation due primarily to low horizontal resolution. These studies also show reduced biases in CCM2 polar simulation due to the use of the semi-Lagrangian water vapor transport and to higher horizontal resolution. CCM2 midlatitude simulation is generally poor, however, due to unrealistic cloud radiative properties (Kiehl et al. 1994). Following these studies, the present paper assesses the polar simulation of CCM3.

In a companion paper Briegleb and Bromwich (1998), the focus is on the polar radiation budgets of CCM3. While it may seem desirable to confine the CCM3 polar simulation assessment to one paper, a comprehensive treatment considering radiative, dynamic, and hydrologic aspects for both poles is quite an undertaking. Reference to the CCM3 simulation papers just mentioned shows that even for the Tropics and midlatitudes, a separation of energy, dynamic, hydrologic, and land simulations of CCM3 was necessary. This paper thus completes the assessment of the CCM3 polar simulation by focusing on the polar circulation, thermodynamic structure, and hydrology of CCM3.

To assess the polar climate of CCM3, we compare seasonal and annual means of several meteorological fields with available observations and analyses, with an emphasis on the lower troposphere and surface simulation important for coupling in CSM. The simulation of seasonal and annual sea level pressure (SLP) and associated 500-hPa height shows how well CCM3 responds to high-latitude zonally asymmetric orographic and thermal forcings. The depth and shape of the polar vortex shown by the 500-hPa heights indicate midtropospheric flow and lower tropospheric mean temperature. SLP indicates how well CCM3 simulates the near-surface circulation important for coupling to ocean and sea ice components. Polar regions commonly have strong low-level temperature inversions, especially in winter, and the magnitude of the CCM3 inversions indicate its response to lower atmosphere and surface heat fluxes. The general dryness of polar atmospheres, as shown by the precipitable water (PW), is an important factor in cloud formation and in radiation–precipitation processes. Net freshwater flux at the surface (precipitation minus evaporation, or $P - E$) is an important measure of CCM3's transport, hydrologic, and evaporation simulation. Finally, we consider the surface heat balance of CCM3.

Data for the validation of CCM3 polar climate are taken from several sources. The most important are two European Centre for Medium-Range Weather Forecasts (ECMWF) analysis datasets from within the 1979–93 period of the CCM3 integration. It is readily acknowledged that while these datasets represent some of the best collections of gridded meteorological data available, they often have significant biases (e.g., Cullather et al. 1997). Conservative estimates of uncertainties in analyses and other observations will be made with the best available information. Without such estimates, the significance of differences between CCM3 and analysis/observations is difficult to determine.

The paper is organized as follows. Section 2 gives a brief description of the CCM3 physics appropriate for polar processes, as well as the analyses and obervations used for the comparison. In section 3, the CCM3 polar simulation and analyses/observations are compared. Section 4 concludes with a summary.

2. Model and analyses/observations

a. Model

The most recent version of the NCAR Community Climate Model is version 3 (CCM3). A general description of CCM3 is found in Kiehl et al. (1998a), while a complete description of the physics and numerical approximations is found in Kiehl et al. (1996). CCM3 includes several improvements over CCM2, although many aspects of the model formulation are identical to those of CCM2. The standard version of CCM3 has horizontal resolution of T42 (triangular truncation at wavenumber 42, about 2.8° lat × 2.8° long) with the same 18 vertical hybrid coordinate levels as in CCM2. CCM3 continues to employ the semi-implicit/leapfrog time integration scheme, spectral transform method for treating the dry dynamics, a biharmonic horizontal diffusion operator, and a semi-Lagrangian scheme for transporting water vapor. Modifications to the physical parameterizations of CCM2 were motivated both by the desire to reduce its systematic simulation errors, particularly in top-of-atmosphere and surface energy budgets, as well as to make the model more suitable for coupling to alternative surface (land, ocean, ice) component models.

As just noted, the atmospheric transport of water vapor into high latitudes is evaluated by the semi-Lagrangian method (in contrast to the less accurate spectral transport method, used in CCM versions prior to CCM2). The semi-Lagrangian method uses a rotated spherical coordinate near the poles, which passes an equator through the particle departure point, to avoid numerical inaccuracies due to converging meridians. Precipitation occurs in two forms: stable and convective.

When the column is stable to moist convection, only stable precipitation occurs whenever saturated conditions exist. Low-level evaporation of stable precipitation is allowed in CCM3. The phase of precipitation for surface accumulation depends on low-level temperature. Convective precipitation occurs when the column is unstable to moist convection. These precipitation processes are mostly independent of the cloud prediction scheme and of the radiative properties of the clouds.

The diagnostic cloud fraction depends on relative humidity, vertical motion, and boundary layer stability. Cloud water path is a function of total column precipitable water. Cloud particle optical properties vary with phase. Cloud particle size depends on surface type (ocean and land) and on atmospheric pressure (see Briegleb and Bromwich 1998).

Exchange of surface fluxes with the lower atmosphere is moderated through the planetary boundary layer. The boundary layer is resolved reasonably well by the first six atmospheric levels over the surface, whose pressures (as fractions of the surface pressure) are 0.990, 0.962, 0.920, 0.862, 0.789, and 0.701. This means that the lowest free atmospheric level is about 10 hPa above the ocean surface, or at about 80-m elevation.

CCM3 employs a nonlocal boundary layer diffusion scheme that accounts for countergradient fluxes under unstable conditions for which the length scale of the largest turbulent eddies may be that of the boundary layer depth itself. Under neutral and stable conditions, the boundary layer diffusion is local. The bulk formulas for surface flux exchange over land are those from the land surface model (LSM, Bonan 1996), while over ocean they are identical to those employed in the CSM (Kiehl et al. 1996). Using identical bulk formulas over ocean and sea ice in both CCM3 and in CSM reduces climatological drift in coupled simulations. The surface exchange coefficients over ocean and sea ice are stability dependent, and in particular the stress depends quadratically on the surface wind speed.

Over land, the surface conditions are represented by the LSM of Bonan (1996). Snow is determined by a simple mass balance between gains from snowfall and surface deposition of vapor to liquid and to solid, and losses from snow melt and sublimation. The horizontal fraction of ground covered with snow is proportional to the snow mass for snow depths below 5 cm, above which the fraction is one.

Over ocean the prescribed surface temperatures are linearly interpolated between monthly mean values. Whenever the sea surface temperature (SST) is less than the minimum −1.8°C, sea ice conditions are assumed. Sea ice is represented by a constant thickness slab of 2-m water ice that completely covers the ocean grid box, overlain with a constant uniform layer of 0.005 m (liquid water equivalent) snow, with initial ice temperatures at freezing. The ice temperatures are then computed using a four-layer diffusion model with constant layer thicknesses of 50 cm and a constant ocean lower boundary freezing temperature, thus allowing for heat exchange with the underlying ocean. The top layer snow–ice mixture assumes snow overlying ice and distinguishes the thermal conductivities of snow and ice. The top layer ice temperature is used to compute surface flux exchange with the atmosphere. Surface aerodynamic roughness of ice is constant. Sea ice–snow composite albedos allow for partial coverage of the ice by overlying snow, but are constant in time. In particular, they are independent of temperature (i.e., no summer melt ponds).

The CCM3 polar climates discussed in this paper are those simulated by an integration from January 1979 through August 1993, known as the Atmospheric Model Intercomparison Project integration (AMIP, Gates 1992). This AMIP integration prescribes monthly mean SSTs and implied sea-ice distribution as ocean boundary conditions for CCM3. As noted above, the sea-ice distribution is implied by the lowest SSTs in this dataset. The seasonal and interannual representation of sea-ice extent in this AMIP SST dataset is shown in Briegleb and Bromwich (1998). Year-to-year variations in ice are confined to ice extent (not ice concentration, thickness, type, or surface albedo).

b. Analyses/observations

The analyses and observations used for assessing the CCM3 polar climate simulations were taken from a variety of sources. ECMWF analyses for the periods 1980–89 (WMO initialized archive) and 1985–92 (uninitialized WCRP/TOGA Archive II) were used. Monthly mean ECMWF 1980–89 surface pressures were available on the CCM T42 Gaussian grid (Trenberth 1992). Differences between 1980–89 and 1985–92 SLP are minimal. Because of the analyses changes in the hydrologic cycle before May 1985, the period 1985–92 of the WCRP/TOGA Archive II analyses was considered better for comparison of hydrologic fields. In addition, some surface quantities were not available from the WMO 1980–89 analyses. Seasonal means were computed using the 9 (northern) winters and 10 (northern) summers from 1980–89. Estimates of uncertainties in the analyses are given when compared with CCM3 (see next section).

For SLP, the method of Trenberth et al. (1993) was used to reduce surface pressure to SLP for both model and analyses. Monthly mean surface temperatures (T_s) are employed to reduce the surface pressure at the model's geopotential surface height to sea level assuming a constant 6.5°C/km lapse rate. It was found necessary to use a mean temperature (K) of $\frac{1}{2}(240 + T_s)$ for cold elevated surfaces to prevent unduly high SLPs. The CCM3 surface air temperature was used for the ECMWF SLP calculation, as analysis surface temperature during 1980–89 was not available. Interannual variability (standard deviation, or σ_{SLP}) was computed based on individual annual means.

(a)

DJF CCM3 500 hPa Height

1980–1989   (m)

CONTOUR FROM 4950 TO 5650 BY CONTOUR INTERVAL 50

(b)

DJF ECMWF 500 hPa Height

1980–1989   (m)
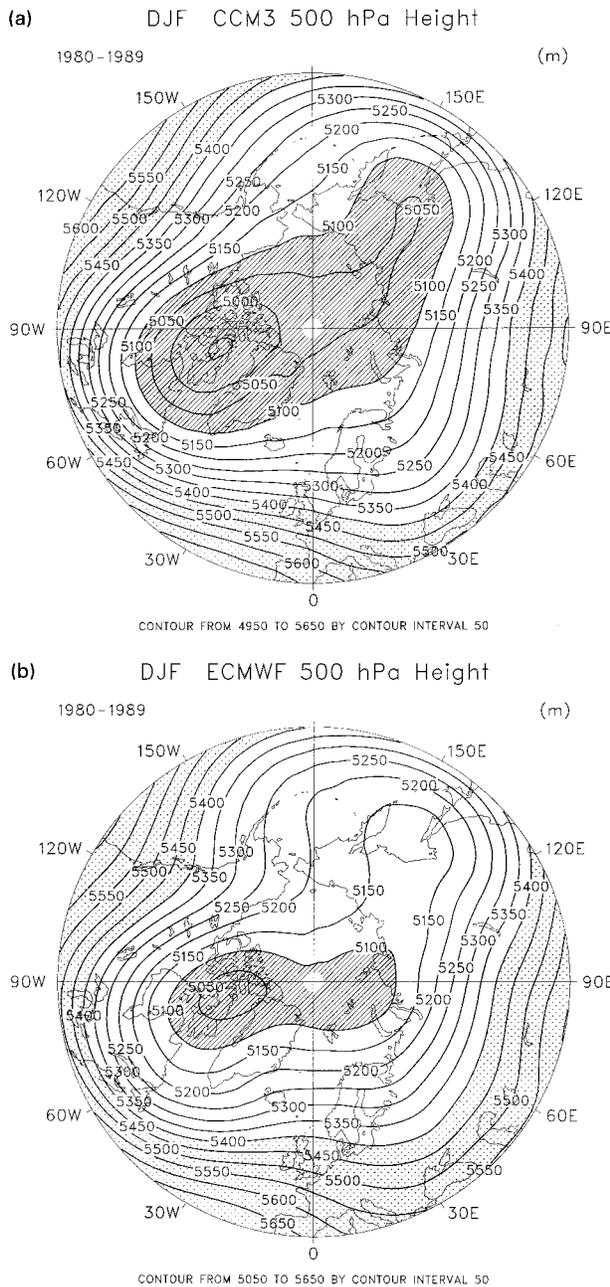
CONTOUR FROM 5050 TO 5650 BY CONTOUR INTERVAL 50

FIG. 1. Ensemble winter season [December–February (DJF)] Arctic 500-hPa geopotential height field for (a) CCM3 AMIP integration (1980–89), and (b) ECMWF WMO analyses for the same period, contoured every 50 m, with regions less than 5100 m hatched, and regions greater than 5400 m stippled.

3. Assessment of CCM3 polar simulation

a. Arctic

1) 500-HPA HEIGHT

The winter polar vortex of CCM3 is compared with that of the ECMWF analyses (1980–89) in Figs. 1a,b, as indicated by the 500-hPa height field. Differences
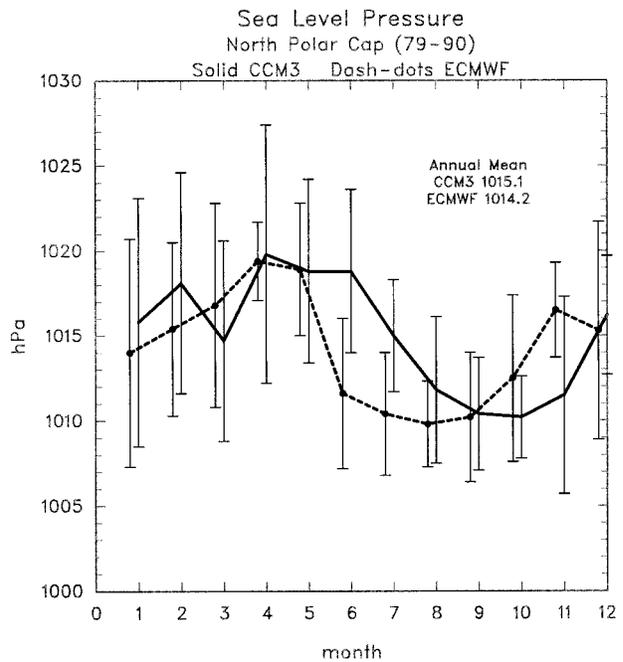
Sea Level Pressure
North Polar Cap (79–90)
Solid CCM3   Dash–dots ECMWF

Annual Mean
CCM3 1015.1
ECMWF 1014.2

FIG. 2. Annual run of ensemble (1980–89) monthly polar cap (79°–90°) mean SLP, CCM3 AMIP integration (solid), and ECMWF WMO analyses (dash–dot). Error bars are plus/minus interannual monthly standard deviation of the 10 yr of monthly means. The analyses are offset in time for readability.

larger than ± 25 m (about $\pm 1°C$ in mean temperature) can be considered significant, since systematic errors in temperature greater than $\pm 1°C$ in the lower troposphere are not likely. The winter polar vortex of CCM3 is positioned with a minimum height over Baffin Island as in the analyses, but it is too zonally symmetric and too deep by 50–100 m. This means that lower tropospheric mean temperatures are colder by 2°–4°C, and that mid-tropospheric winds are stronger than those of the analyses. Asymmetric regions of low heights at a particular latitude (troughs) over east North America, Europe, and East Asia are well positioned in longitude, while the higher height regions in between them (ridges) are not as well simulated. Differences (not shown) disclose a wavenumber 2 pattern around 60°N. The summer polar vortex (not shown) likewise is too zonally symmetric and too deep by 50 m, but is well centered over the pole. This deep polar vortex is associated with colder lower troposphere temperatures (see below) and stronger tropospheric winds than in the analyses. It is noteworthy that the CCM3 Arctic top-of-atmosphere annual radiation budget is several Watts per square meter less than the observations (Briegleb and Bromwich 1998).

2) SEA LEVEL PRESSURE

Figure 2 shows the annual cycle of central Arctic SLP, averaged over 79° to the pole. Also shown are the interannual monthly standard deviations (σ) of the 10 yr

(a)   Annual CCM3 Sea Level Pressure

(b)   Annual ECMWF Sea Level Pressure

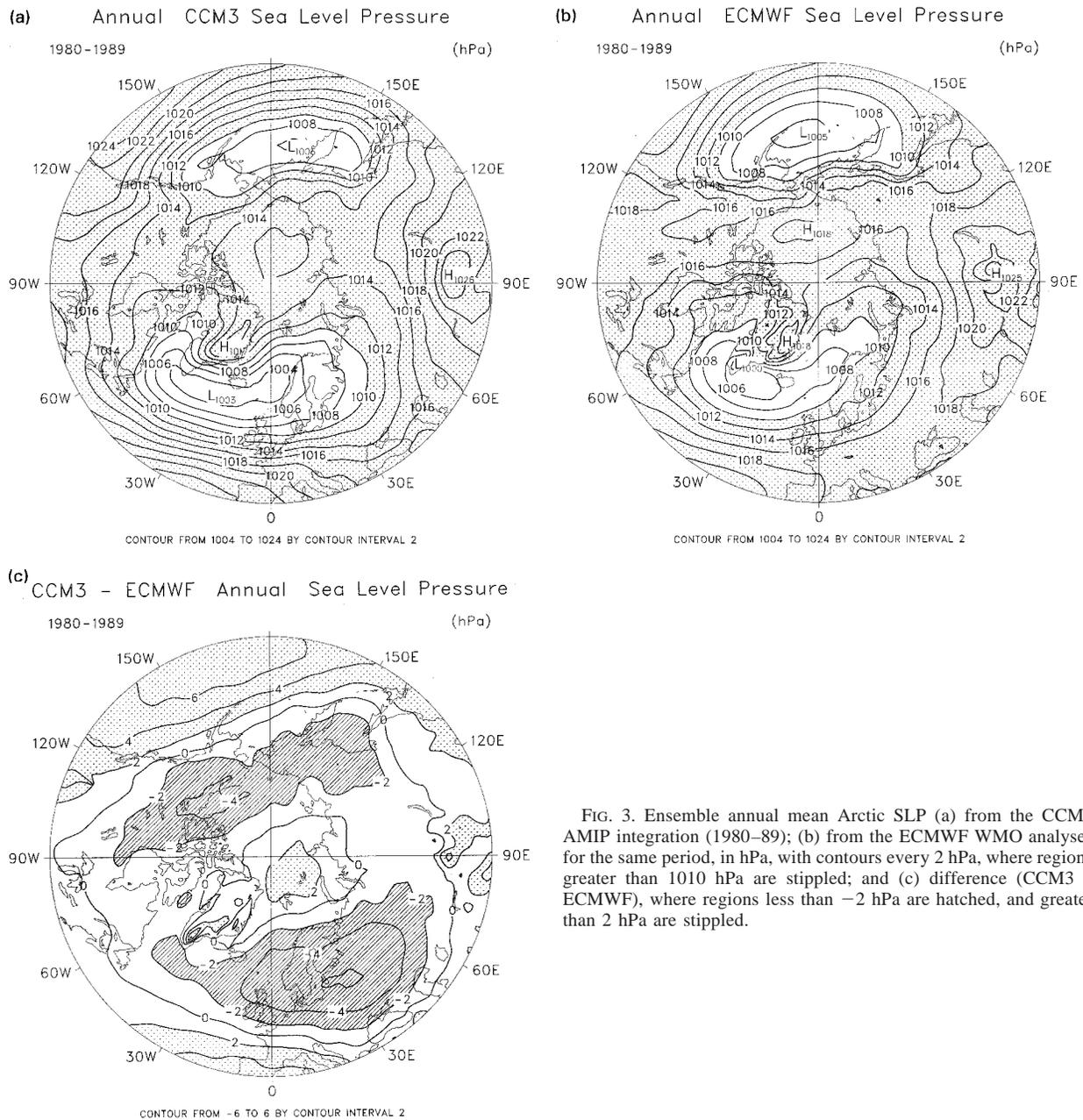**(c)** CCM3 – ECMWF Annual Sea Level Pressure

FIG. 3. Ensemble annual mean Arctic SLP (a) from the CCM3 AMIP integration (1980–89); (b) from the ECMWF WMO analyses for the same period, in hPa, with contours every 2 hPa, where regions greater than 1010 hPa are stippled; and (c) difference (CCM3 – ECMWF), where regions less than −2 hPa are hatched, and greater than 2 hPa are stippled.

of data (monthly value $\pm\sigma$), ranging from 2 to 7 hPa. Differences larger than ±2 hPa are likely to be significant, since interannual variations in SLP (discussed below) are typically around 2–3 hPa. It appears that the phase of CCM3 mean SLP is delayed by 1–2 months compared to the ECMWF analyses. This could be related to the lack of seasonal snow melt and melt pond effects on sea-ice albedo, as well as to the prescribed 100% sea-ice concentration. CCM3 summer SLP around the Arctic (not shown) has continental heat lows and midlatitude oceanic highs as in the analyses, although the latter are 5 hPa too high. There is rough correspon-

dence between CCM3 and ECMWF monthly interannual variability, although CCM3 has comparable or even larger variability than the analyses.

Figures 3a–c compare the Arctic mean annual SLP for CCM3 with the ECMWF analyses. Note how the Arctic Ocean sea level pressure maximum (or high) is displaced poleward, while the Icelandic region minimum (or low) is extended toward Europe, and the Aleutian region minimum (or low) is extended toward Asia. The Aleutian low pressure region shows evidence of the split center so prevalent in CCM2 (Bromwich et al. 1994). The poleward displaced Arctic high results in

increased cyclonic circulation in the Beaufort Sea and increased anticyclonic circulation in the European sector of the Arctic basin. The smoothed Greenland and Norwegian topography may be distorting flow in this region, biasing the SLP pattern. Also noteworthy is the increased cyclonic circulation in northern Europe and the increased anticyclonic circulation in the North Pacific. The SLP differences of Fig. 3c shows evidence of large-scale extratropical patterns. The implications of these patterns will be discussed further in the concluding section.

The SLP annual variability (σ_{SLP}, not shown) indicates the ability of CCM3 to respond to varying SST forcings, as well as to simulate the intrinsic internal variablity of the atmosphere. ECMWF SLP variability is small over most land surfaces (<1 hPa), while maximizing around 2.5–3.0 hPa in the Gulf of Alaska and in the European sector of the Arctic basin. CCM3 SLP variability is roughly comparable in position, though slightly larger in magnitude (3.0–4.0 hPa). CCM3 and ECMWF SLP variability are similar in magnitude and pattern to that shown in Power and Mysak (1992), based on surface SLP observations from 1952 to 1987.

3) SURFACE STRESS

CCM3 mean annual Arctic surface stress was examined. The magnitudes of the stress range from 0.02 to 0.05 N m^{-2} in the central Arctic, to 0.20 N m^{-2} in the east Greenland current. The magnitudes and directions of the surface stress approximately follow the isobars of SLP, being slightly turned to the left (about 20°–30° in angle) as would be expected. There is less CCM3 surface flow from Asia toward Fram Strait than that indicated by the ECMWF SLP. The surface stress in the central Arctic shows a large anticyclonic flow that is just closed and is displaced toward the Asiatic side of the Arctic as is the maximum SLP. The implied flow of sea ice forced by this surface stress is thus more centered in the Arctic, rather than toward the Beaufort Sea with a transpolar drift stream as is observed (Weatherly et al. 1998). The katabatic drainage off Greenland looks fairly realistic, given the smoothing effects of the CCM3 T42 resolution (Bromwich et al. 1996).

4) TEMPERATURE

Figure 4 compares air temperature profiles for Resolute, Northwest Territories (NWT), at 75°N, 95°W with available observations. The dashed lines show the mean rawinsonde observations, and the error bars ± the interannual standard deviation (data length is 30 yr from 1960 to 1990). The solid lines are CCM3 ensemble mean (1979–93) January and July profiles for all points within ±3° latitude–longitude of the station. In January, the midtroposphere temperature is in excellent agreement with the observations, while the tropopause is cold. Near the surface, the CCM3 inversion is elevated (i.e., its
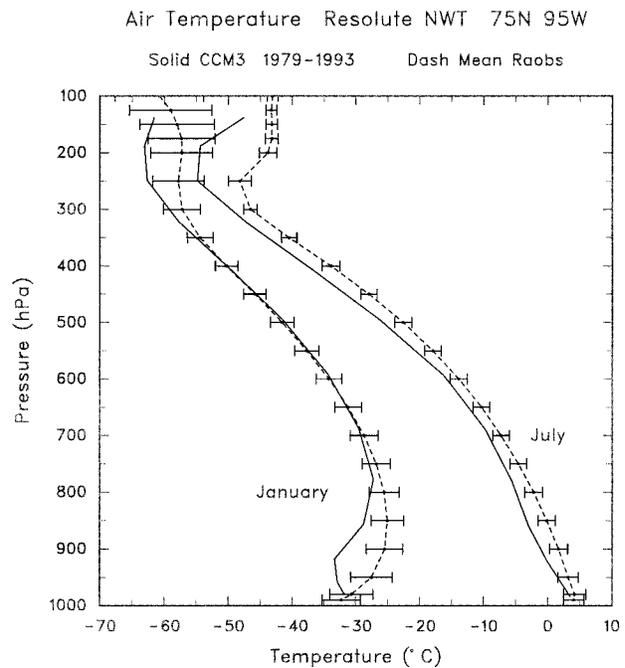

FIG. 4. Air temperature profile for Resolute, NWT (75°N, 95°W), for January and July. Solid is from CCM3 AMIP integration (1979–93), including all grid points within ±3° latitude–longitude of the station. Dashed is the long-term rawinsonde mean, with plus/minus interannual standard deviation as error bars.

base is above the surface), in contrast to the observed surface inversion (i.e., one that is based at the surface). However, the temperature difference across the inversion of about 6°C, as well as the inversion depth of about 1200 m, are comparable to the observations. In July, a uniformly cold (2°–3°C) tropospheric bias exists, while the July tropopause around 200–250 hPa is 6°–10°C cold. CCM3 surface lapse rate is larger than the observations. It is noteworthy that summer absorbed shortwave radiation is significantly less than observed, both at the top of atmosphere and at the surface (Briegleb and Bromwich 1998), consistent with the summer cold bias.

Figure 5 shows a regional map of the CCM3 winter inversion temperature difference (ΔT, temperature difference between inversion base and top within the range from the surface to 500 hPa). Here ΔT is largest (about 6°–8°C) over land adjacent to the Arctic Ocean, but over the central Arctic only 3°–4°C. The values are less than the observed ΔT based on many years of rawinsonde data (Kahl et al. 1992; Serreze et al. 1992), especially over the central Arctic. The observations show typical winter inversions ΔT of 10°–12°C in the central Arctic and adjacent coasts, declining to 5°C or less for more southerly regions. Differences in ΔT larger than 2°–3° are likely to be significant, based on typical interannual station variability (Kahl et al. 1992). Observed inversions are mostly surface based and about 1000–1400 m thick. While CCM3 inversion depth is within this range,
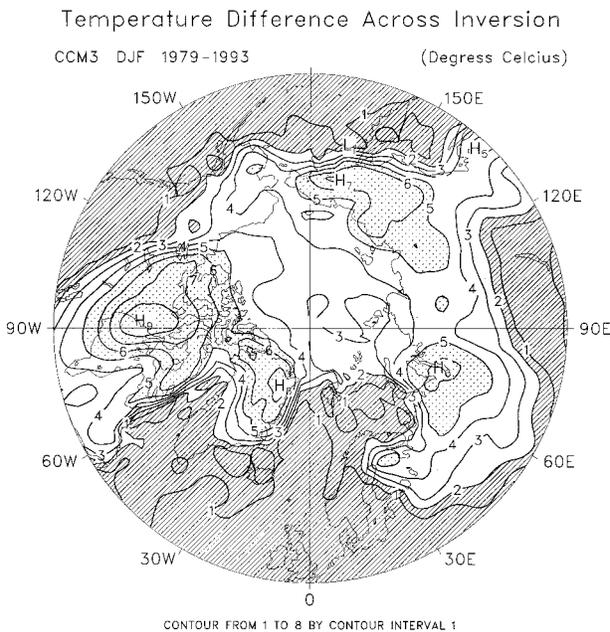
Temperature Difference Across Inversion

CCM3 DJF 1979–1993   (Degress Celcius)

CONTOUR FROM 1 TO 8 BY CONTOUR INTERVAL 1

FIG. 5. Ensemble winter season (DJF) Arctic low-level temperature inversion (°C), from CCM3 AMIP integration (1979–93), defined as the maximum temperature difference in the column from the surface to 500 hPa. Contour interval is 1°C; regions greater than 5°C are stippled, and those less than 2°C are hatched.

Arctic Monthly Surface Air Temperature
Solid = CCM3
Dash/Dots = Station Data

FIG. 6. Ensemble monthly surface air temperature for the Arctic high (85°N, 121°W) in the top panel, the North Greenland Sea (82°N, 17°W) in the middle panel, and for the East Beaufort Sea (77°N, 117°W) in the lower panel. The solid line is from the CCM3 AMIP integration (1979–93) ensemble mean for the closest grid point. The dash line is the ensemble mean (1980–92) data from composite station observations, with plus/minus the interannual standard deviation as error bars. Months are numbered from January (1).

its inversions are elevated to base heights of 700–800 m above the surface. CCM3 winter low-level inversion is thus weak and elevated, though about the observed depth. This is consistent with the results of Briegleb and Bromwich (1998), which show that Arctic winter clouds are too extensive and too optically thick (or emissive). This produces excessive warming of polar surfaces and lower atmosphere, which would tend to erode surface inversions altogether, or at least lift them vertically.

Figure 6 shows the annual cycle of monthly mean surface air temperature for three stations in the Arctic (D. Shea, NCAR, 1996, personal communication). These data were taken from limited surface observations at both nearby land stations and drifting ice stations. Interannual standard deviations are shown for each month. The Arctic surface temperatures in CCM3 are somewhat warm during winter (consistent with elevated inversions) and cold during summer. There appears to be a slight phase shift toward warmer spring and colder fall temperatures. This is consistent with both the uniform 2-m ice thickness with minimal snow cover, and the lack of fractional ice or snow melt and melt ponds on sea ice during summer. The relatively thin ice and minimal snow cover increases heat exchange with the underlying ocean, allowing warmer winter temperatures (typical Arctic sea ice thickness generally exceeds 2 m; see Bourke and Garrett 1987). The lack of snowmelt and melt ponds on sea ice implies lower albedo in spring, and larger albedo in fall, than is observed, implying warmer spring and colder fall temperatures. Brie-
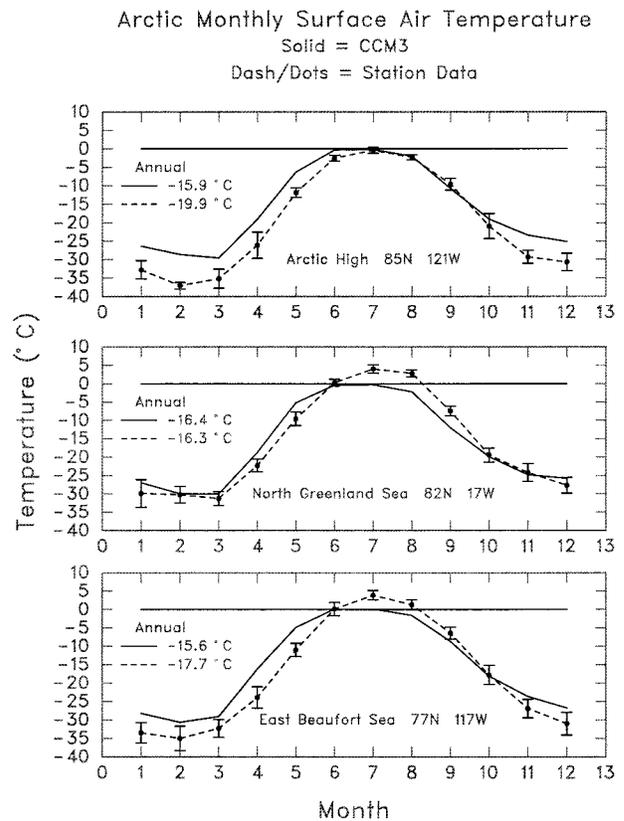
gleb and Bromwich (1998) show that over Arctic sea ice, CCM3 absorbs too much solar radiation in spring and too little in late summer. Note that CCM3 temperatures over sea ice are held below 0°C. On the annual mean, the CCM3 surface temperatures tend to be warm (0°–4°C).

Mean annual surface temperatures for CCM3 and the ECMWF analyses (1985–92) were compared (not shown). The CCM3 surface temperature over ocean is either the water or ice temperature, while over land it is the 2-m air temperature. Annual mean temperature differences larger than ±2°–3°C in high latitudes, reducing to ±1°C by midlatitudes, would be significant. (These are the typical interannual standard deviations of station surface temperature observations.) Europe, East Asia, Alaska, and northern Canada are cold by 1°–2°C, marginally significant, while Greenland highland temperatures are about 5°C warm and smoothed, central Asia is close to the observed, and the central Arctic is warm by 3°–4°C. However, the mean annual comparison misses significant seasonal differences, as shown by

Bonan (1998). In winter, temperatures are 3°–5°C too warm in a region of North America from central Canada northwest to Alaska and in a broad band of Asia extending from the Caspian Sea northeast to far eastern Siberia. In summer, most of northern Europe, Russia, western Asia, Alaska, and northwest Canada are 2.5°–5°C too cold. The warm winter regional land temperatures could be associated with the circulation anomalies noted above, with warm biases in regions adjacent to and downstream of cyclonic anomalies (see Fig. 3c); the cold summer temperatures are consistent with the low summer absorbed shortwave radiation compared to observations (Briegleb and Bromwich 1998).

5) PW AND $P - E$

We compared the annual precipitable water (PW) for both CCM3 and the ECMWF analyses for 1985–92 (not shown). CCM3 PW is uniformly low by 10%–20% compared to the ECMWF analyses. The regional pattern of PW within the dry polar vortex region (Greenland and the Arctic basin) is well simulated. Annual polar cap (70°–90°N) means are 5.8 kg m^{-2} for CCM3 and 6.7 kg m^{-2} for the ECMWF analyses. Serreze et al. (1995) obtained 6.1 kg m^{-2} from radiosonde observations. This uniformly low PW could be related to cold polar tropospheric temperatures, but could also be part of the CCM3 dry moisture bias noted by Hack et al. (1998).

Figures 7a,b compares the annual $P - E$ between CCM3 and the ECMWF analyses. Quantified uncertainty in $P - E$ is not known, but the highly variable nature of P makes close comparison suspect. We estimate regional uncertainties to be at least $\pm 20\%$ of value. The polar desert of the Arctic basin is fairly well simulated; low values of $P - E$ of about 13 cm yr^{-1} in the central Arctic are comparable to those of ECMWF analyses. Regions of very low $P - E$ in the lee of the northern Canadian Rockies, over central Greenland, and in the Norwegian–Barents Sea region, are all simulated by CCM3. The $P - E$ maximum in the western Canadian Rockies, over southern Greenland, and in southern Norway are approximately represented. Annual polar cap (70°–90°N) means are 18.1 cm yr^{-1} for CCM3. This compares favorably with the 18.1 cm yr^{-1} value for the ECMWF analyses, 18.2 cm yr^{-1} for the ECMWF reanalyses from the period 1979–93 (Bromwich and Cullather 1998), and 16.3 ± 0.5 cm yr^{-1} estimated from moisture flux convergence (Serreze et al. 1995).

6) SURFACE ENERGY BUDGET

Nakamura and Oort (1988), (henceforth NO88) inferred the 70°–90°N polar cap net surface heat flux as a residual after accounting for top-of-atmosphere radiative budget, lateral transport across 70°N, and heat storage. Their estimated uncertainty is ± 25 W m^{-2}, a large value because the surface heat flux is a residual of large uncertain terms. The CCM3 polar cap net surface energy

(a) Annual Precipitation – Evaporation
CCM3 1985–1992   (cm/year)

CONTOUR FROM −10 TO 170 BY CONTOUR INTERVAL 10

(b) Annual Precipitation – Evaporation
ECMWF 1985–1992   (cm/year)

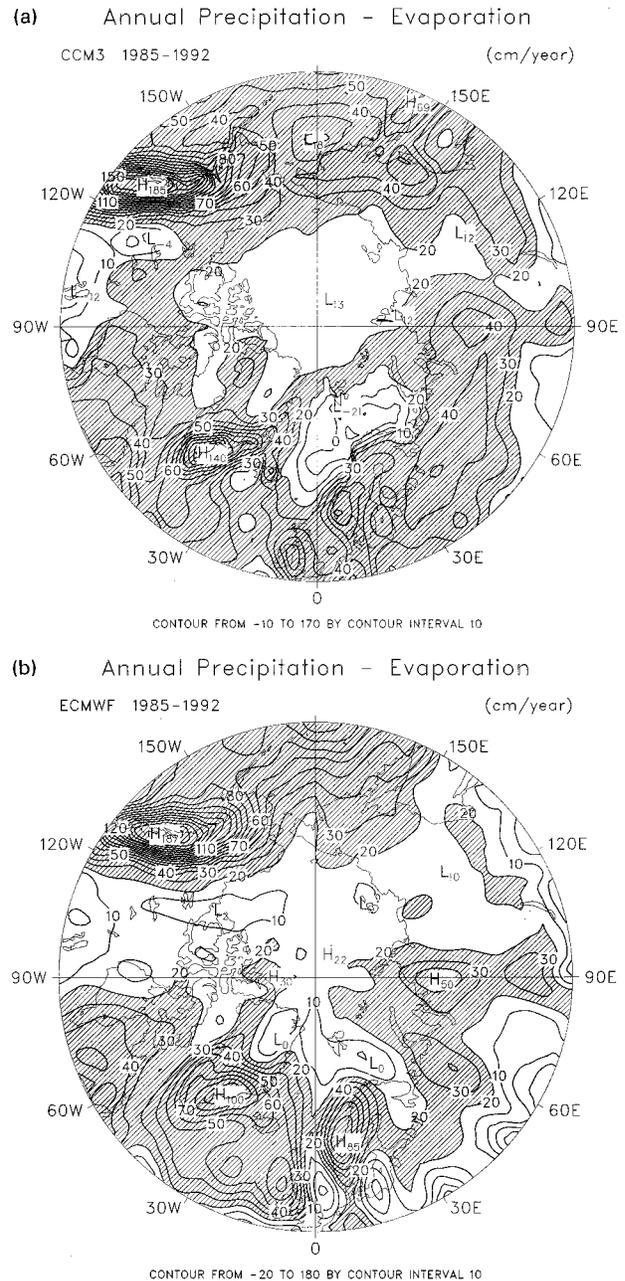CONTOUR FROM −20 TO 180 BY CONTOUR INTERVAL 10

FIG. 7. Ensemble annual Arctic precipitation minus evaporation ($P - E$, cm yr^{-1}) for (a) CCM3 AMIP integration (1985–92), and (b) for ECMWF TOGA Archive II for the same period. Contour interval 10 cm yr^{-1}, and the region greater than 20 cm yr^{-1} is hatched.

flux (positive into surface) was computed for comparison with NO88.

The net surface energy flux is the difference between the absorbed solar flux and the loss of longwave, latent heat, and sensible heat fluxes to the atmosphere. We note that the region of (70°–90°N) includes quite inhomogeneous surfaces, in particular the Arctic basin sea ice and the open ocean in the Barents Sea region. In CCM3, the former annual mean net surface energy flux-

(a)　JJA　CCM3 500 hPa Height

CONTOUR FROM 4750 TO 5550 BY CONTOUR INTERVAL 50

(b)　JJA　ECMWF 500 hPa Height
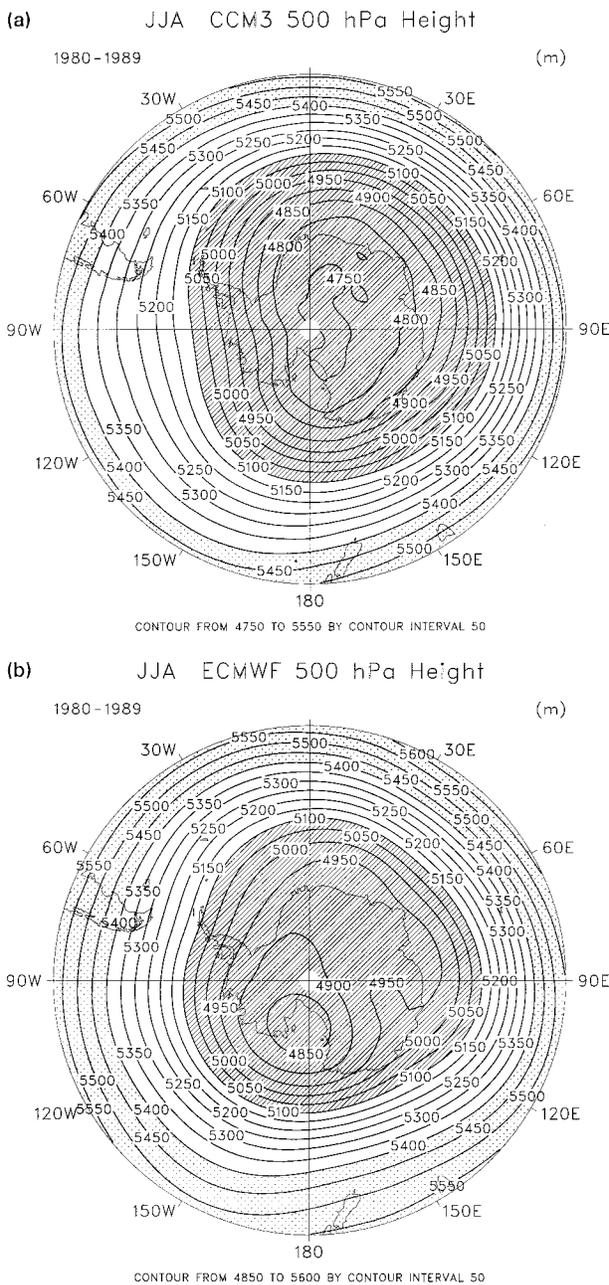

CONTOUR FROM 4850 TO 5600 BY CONTOUR INTERVAL 50

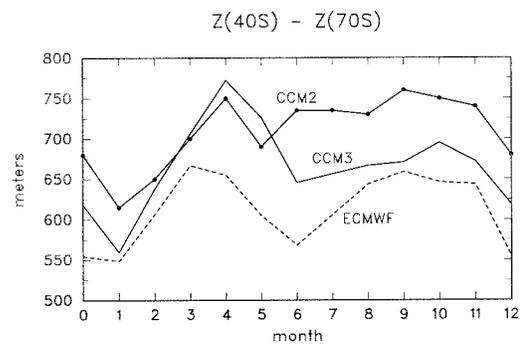FIG. 8. Same as Fig. 1 except for the Antarctic winter (JJA) season. Panels (a) and (b) use 50-m contour interval, with hatching for regions below 5100 m and stippling above 5400 m.

FIG. 9. Ensemble monthly Southern Hemisphere 500-hPa geopotential height difference (40°–70°S). Solid is from CCM3 AMIP integration (1980–89), dash from the ECMWF WMO analyses for the same period, and the solid-dotted line from CCM2 (case 388, 20-yr ensemble mean). Months are numbered from December (0).

es range from about -3 to -7 W m^{-2}, while the latter range from -20 to -120 W m^{-2}.

The polar cap annual mean net surface energy flux for CCM3 is -17.0 W m^{-2}, with December–February (DJF) -47 W m^{-2} and June–August (JJA) 33 W m^{-2}. The estimates from NO88 are annual -2.4 W m^{-2}, DJF -48 W m^{-2}, and JJA 67 W m^{-2}. The CCM3 JJA value is 34 W m^{-2} less that NO88, which is probably a significant difference. We note that Briegleb and Bromwich (1998) showed that CCM3 JJA top-of-atmosphere solar

absorbed flux was smaller than satellite observations by 24 W m^{-2}, a comparable number. We estimate that the CCM3 JJA net surface energy flux is low by about 20 W m^{-2}.

b. Antarctic

1) 500-HPA HEIGHT AND TROPOSPHERIC WINDS

The winter (JJA) polar vortex of CCM3 is compared with that of the ECMWF analyses (1980–89) in Figs. 8a,b, as indicated by the 500-hPa height field. The center of the CCM3 vortex is shifted from the Ross Sea to over the South Pole. The trough and ridge pattern in the Western Hemisphere is rotated westward about 30°, differing typically from 50 to -50 m compared to the analyses. The Eastern Hemisphere is too deep in general by 100–150 m, and the ridges at 45° and 150°E with the intermediate trough at 100°E are not represented by CCM3, whose pattern is very zonally symmetric. These height differences are significant. As with the Arctic, the CCM3 Antarctic top-of-atmosphere annual radiation budget is several Watts per square meter less than the observations (Briegleb and Bromwich 1998).

The strong polar vortex of CCM3 (i.e., very low 500-hPa height) indicates that its midtropospheric winds from 40° to 70°S are stronger than the analyses. The mean 500-hPa geostrophic zonal wind in this latitude range is proportional to the zonally averaged difference in height. The latter is shown on Fig. 9, for CCM2, CCM3, and the ECMWF analyses. The annual and semiannual march of CCM3 geostrophic winds is consistent with the analyses, though larger in magnitude. The strongest CCM3 zonal winds occur in April and May, the months of the lowest circumpolar trough SLP (see Fig. 11, which is discussed below).

As was noted in Tzeng et al. (1994), CCM2 was able to reproduce the split jet stream in the middle and upper troposphere over the Pacific and Indian Oceans during winter (July). CCM3 is also able to reproduce the split jet stream (not shown) in a manner similar to CCM2.

If anything, the overall pattern of zonal wind speed at 300 hPa in July is closer to the analyses shown in Tzeng et al. (1994) than is CCM2. The core minimum zonal wind at 180°E next to New Zealand has a wind speed of 16.9 m s^{-1}, compared to that of 19.4 m s^{-1} of CCM2 and 12.3 m s^{-1} of the ECMWF analyses. This split jet stream is important for Pacific sector ENSO variability as discussed in Chen et al. (1996).

2) SEA LEVEL PRESSURE

In Figs. 10a–c we compare the annual mean SLP of CCM3 with the ECMWF analyses. The CCM3 circumpolar trough is deeper in some regions than the analyses by 3–4 hPa and is shifted northward in position. This northward shift might be partially caused by the smoothed Antarctic topography, and therefore on the horizontal resolution of CCM3 (see concluding section). The stronger cyclonic circulation implied by Fig. 10c at 60°S and 45°E, 170°E, and 60°W means CCM3 midlatitude surface westerlies and polar easterlies are stronger than in the analyses. While the reduction to sea level pressure over the Antarctic continent introduces large uncertainties, it is noteworthy that CCM3 SLP is also less than the analyses over the continent by several hPa.

Figure 11 compares the monthly zonal mean circumpolar trough strength (given by the minimum zonal mean SLP), between CCM2, CCM3, and the ECMWF analyses. Values larger than 2 hPa are likely to be significant. CCM2 has uniformly low trough strength, (annual mean 5.7 hPa lower than the analyses), and only a weak suggestion of a semiannual oscillation. CCM3 trough strength, while still too low (annual mean 2.3 hPa lower than the analyses), shows a semiannual oscillation nearly in phase with the analyses, although the transitional seasons of fall and spring are too deep, and the fall (March–April) phase is delayed by one month. Circumpolar trough position can only be roughly estimated, as the latitudinal resolution of the CCM3 is 2.8° compared to 2.5° of the ECMWF analyses. The trough minimum in CCM3 occurs around the latitude 62°S, somewhat north of that of the ECMWF analyses at 65°S.

The annual SLP variability σ_{SLP} (not shown) indicates the ability of CCM3 to accurately respond to varying SST–sea-ice forcings, in particular, those related to the El Niño–Southern Oscillation (ENSO) phenomenon, which are known to be correlated with the variability in the South Pacific sector 120°W–180° (Cullather et al. 1996; Chen et al. 1996). CCM3 σ_{SLP} has maximum values of 2–2.5 hPa in the Southern Ocean Western Hemisphere at 55°S and 120°W in rough agreement with the analyses. The Southern Ocean Eastern Hemisphere has smaller interannual variability (1–2 hPa), with smaller maxima at (60°S, 0°) and (60°S, 90°E), of 1.5–2.0 hPa, in rough agreement with the analyses. In general, CCM3 variability is less than that of the analyses by 0.5 to 1 hPa. The CCM3 West Antarctic variability is consistent with that shown in Cullather et al. (1996) in which the

trough minimum position varies between the Ross and Amundsen Seas, while the troughs in East Antarctica maintain their approximate position but vary slightly in strength. This was verified by examination of individual annual SLP maps.

3) SURFACE WINDS AND STRESS

Surface winds in the Southern Ocean generally follow the SLP isobars, turned somewhat to the right (by 20°–30° in angle), as the circumpolar trough is an area of low-level convergence of the southward midlatitude westerly flow and the northward katabatic wind flow from the Antarctic continent. Figure 12 shows the winter (JJA) lowest atmospheric level (about 80-m elevation) CCM3 wind. Over the Antarctic continent, the katabatic wind flow is well represented by CCM3. The Antarctic katabatic wind regime is a thermally direct circulation driven by strong surface radiative cooling and is confined to the lowest 300 m over the surface. The katabatic winds flow primarily downslope, with minimum wind on the topographic height crest of East Antarctica. It is not too surprising that the CCM3 surface winds are fairly accurate in general direction and magnitude, since the surface temperature inversion is well simulated (see below), and to first order, the katabatic wind speed is proportional to the product of inversion strength and terrain slope (Tzeng et al. 1994). The convergence zone at the source of the Ross Ice Shelf, the outflow along the Antarctic coast, and the jet near the Amery Ice Shelf (70°E) are well simulated. The wind speeds near the coast are about the 10 m s^{-1} reported in Tzeng et al. (1994). One might expect that these wind speeds would be larger than observed, given the strength of the polar vortex, but the 80-m wind level combined with highly variable nature of the observed winds make a quantitative comparison difficult.

Of interest for ocean and sea-ice forcing is the surface wind stress. Coastal katabatic wind stress magnitudes range from 0.1 to 0.3 N m^{-2}, while typical midlatitude (45°S) stresses are from 0.1 to 0.2 N m^{-2}. Low values of 0.05 N m^{-2} exist within the circumpolar trough itself (i.e., for SLP less than 980 hPa). Differences in SLP between CCM3 and the ECMWF analyses imply differences in surface wind stress. A sensitivity calculation was performed to estimate the potential bias in CCM3 surface stress implied by the SLP differences. An effective exchange coefficient was evaluated using CCM3 surface stresses and surface geostrophic winds from the CCM3 SLP, with typical values from 1 to 5×10^{-3}. This effective exchange coefficient was used along with surface geostrophic winds from the ECMWF SLP to compute an effective ECMWF surface stress. The change in geostrophic wind was about 10%–20% magnitude decrease, and the resulting quadratically dependent zonal stress decreased by about 60% for the maximum westerly zonal stress around 50°S, and by about 80% for the maximum easterly zonal stress around 70°S.

(a)   Annual CCM3 Sea Level Pressure
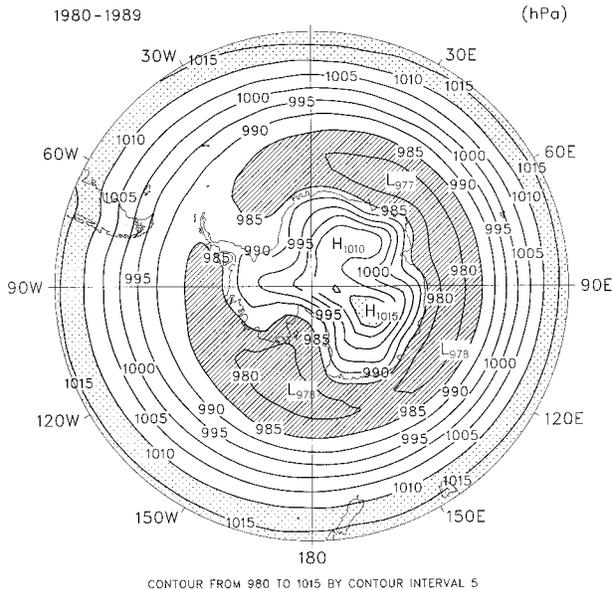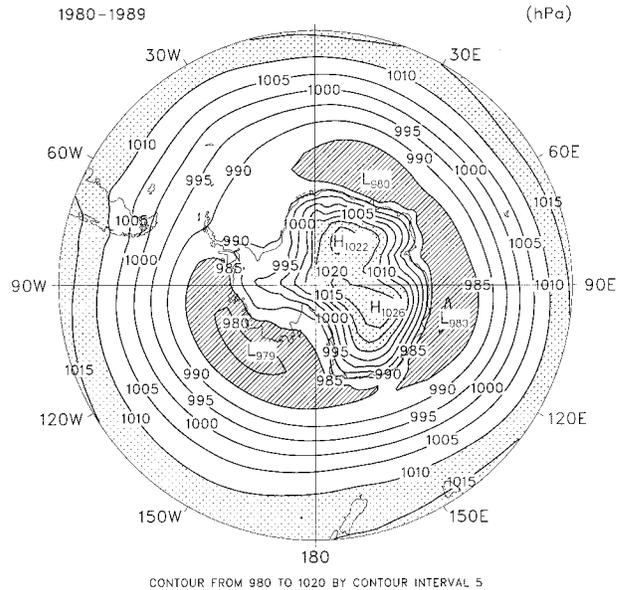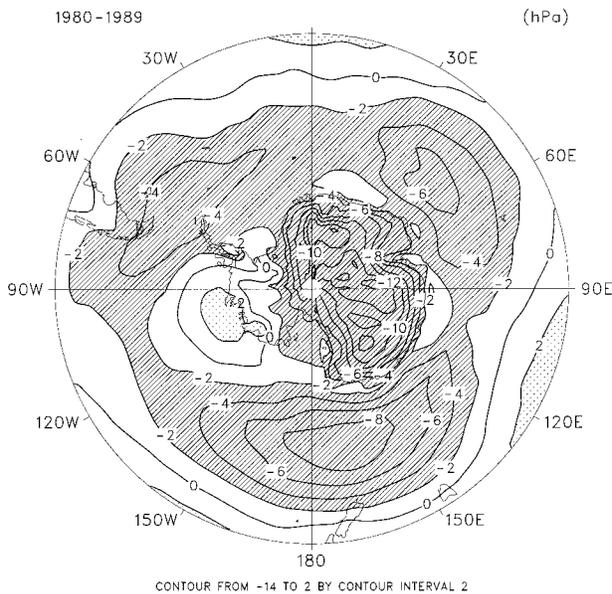
(b)   Annual   ECMWF Sea Level Pressure

FIG. 10. Same as Fig. 3 except for the Antarctic. For (a) and (b) contour interval is 5 hPa, with hatching for regions less than 985 hPa, stippling for regions greater than 1010 hPa.

(c) CCM3 – ECMWF Annual Sea Level Pressure

These potential changes in wind stress are likely to be significant. Thus, if the CCM3 SLP pattern was identical to the ECMWF SLP pattern, one would expect a (conservative) reduction in atmosphere–ocean surface stress of 30%–50%.

Another source of bias in CCM3 surface stresses is the large aerodynamic roughness of sea ice (0.04 m) employed. This value was taken from typical land-ice values for CCM2 and carried into CCM3. Reducing this value to 0.0005 m for sea ice would bring the air drag coefficient close to observed values (Weatherly et al.

1998) and therefore (other factors equal) reduce the atmosphere–ice stress by about 50%.

4) TEMPERATURE

Figures 13a,b compare air temperature profiles for January and July, for two Antarctic locations, with available observations. For McMurdo Station in Fig. 13a, during July (the local winter), the upper tropospheric temperatures are well simulated (except for a cold tropopause), but near the surface there is too strong an
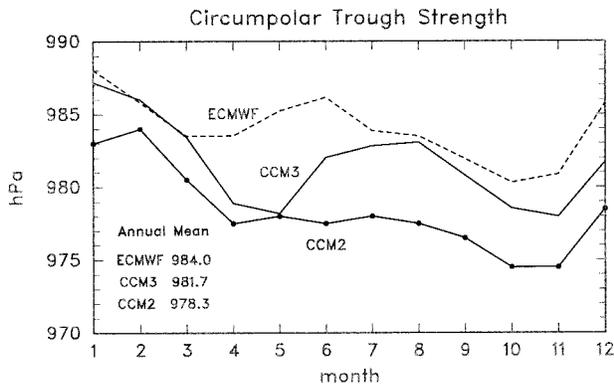
FIG. 11. Antarctic circumpolar trough strength, given as the ensemble monthly zonal minimum SLP. Solid is from the CCM3 AMIP integration (1980–89), dash from the ECMWF–WMO analyses for the same period, and the solid-dotted line from CCM2 (case 388, 20-yr ensemble mean).

inversion (nearly 13°C). This shows that CCM3 is unable to simulate the observed horizontal gradient of 2-m air temperature of 10°C within 100-km distance toward the Ross Ice Shelf (Savage and Stearns 1985). January shows a mild warm bias in the lower troposphere, while the cold bias at the tropopause is very large. The tropopause is about 50 hPa too high and well over 10°C too cold.

Figure 13b compares profiles for the South Pole. In July, the tropospheric temperature profile is well simulated, although the low-level temperature inversion is slightly elevated. In January, a distinct cold bias of 3°–6°C exists, with the near-surface isothermal layer well
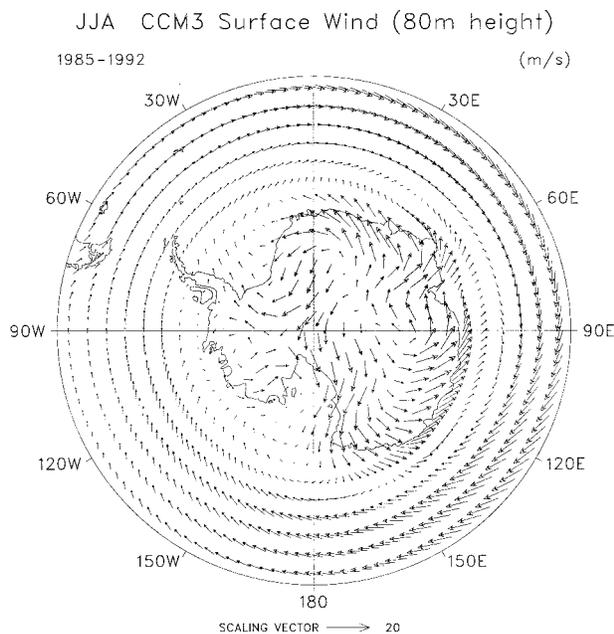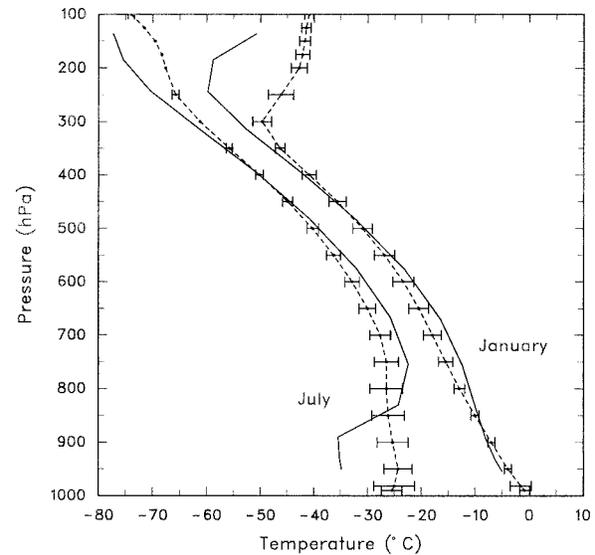

FIG. 12. Ensemble winter (JJA) Antarctic surface (about 80 m) wind (m s⁻¹) for CCM3 AMIP integration (1985–92). Scaling vector is 20 m s⁻¹.
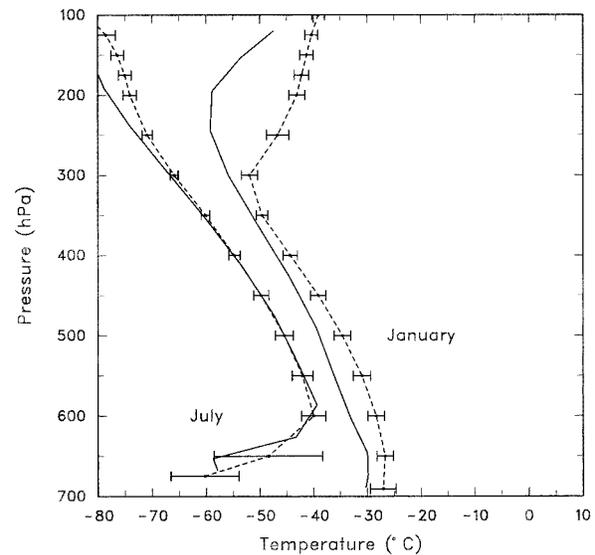

FIG. 13. Same as Fig. 4 except (a) for McMurdo Station (78°S, 167°E) and (b) for the South Pole.

represented. Again, the strikingly cold tropopause is evident, similar to that at McMurdo Station.

Figure 14 shows the winter low-level temperature inversion ΔT over Antarctica in CCM3. The ΔT of 25° to 30°C are found in the East Antarctic plateau, gradually diminishing toward the coasts. Compared to available observations (Tzeng et al. 1994) the inversion maxima over the East Antarctic plateau are about 5°C stronger than observed, which is somewhat significant. The

Temperature Difference Across Inversion

CCM3 JJA 1979-1993   (Degress Celcius)
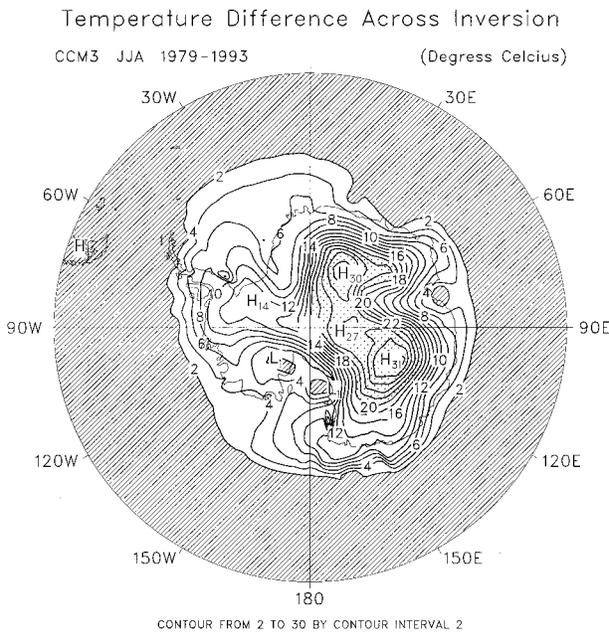

CONTOUR FROM 2 TO 30 BY CONTOUR INTERVAL 2

FIG. 14. Same as Fig. 5 except for Antarctic winter season (JJA). Contour interval 2°C; regions greater than 20°C are stippled, and those less than 2°C are hatched.

Antarctic Monthly Surface Air Temperature
Solid = CCM3 With Dots = Topographically adjusted
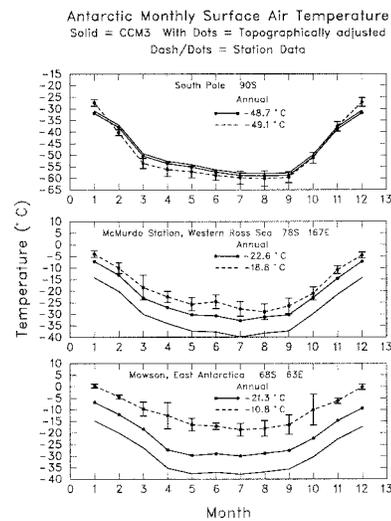Dash/Dots = Station Data

FIG. 15. Same as Fig. 6 except for three stations in the Antarctic: (top) the South Pole, (middle) McMurdo Station (78°S, 167°E), and (lower) Mawson (68°S, 63°E). The solid-dotted lines are the topographically adjusted surface air temperature using 1°C/100 m lapse rate. Station data from long-term surface observations, nominally from 1960 to 1990.

inversion enroaches over the coastline into the surrounding coastal waters in many cases (note Fig. 13a for July). The coastal inversion is larger than observed primarily from 130° to 170°E, similar to CCM2. The CCM3 inversion is near surface (within 100 m) over most of the continent, being elevated up to base heights of several hundred meters over sea ice. Inversion thickness ranges from 800 to 1500 m.

A strong determinant of the magnitude of the inversion is the surface radiative cooling. As shown in Briegleb and Bromwich (1998), clear sky downward longwave is too small in CCM3, but this is mostly compensated by winter clouds that are too extensive and somewhat too emissive. The result is a surface radiative cooling slightly in excess of observations. Thus, the low-level temperature inversion is being driven by about the right surface radiative cooling.

Figure 15 shows the annual cycle of monthly mean surface air temperature for three stations in the Antarctic. Also shown are the surface air temperatures adjusted to the same altitude as the actual topography using a representative lapse rate along the snow surface of 1°C/100 m (Tzeng et al. 1993). These data were taken from surface station climatologies. The coastal stations (lower two panels) show low temperatures (combined with too strong a temperature inversion) while the temperature at the South Pole is close to the observed. Note that the monthly temperature differences, which are moderately significant, are in the same sense as that for the Arctic—somewhat warm in winter but cold in summer. The coastal stations are cold even when the topographic height adjustment is included. Recall that CCM3 has
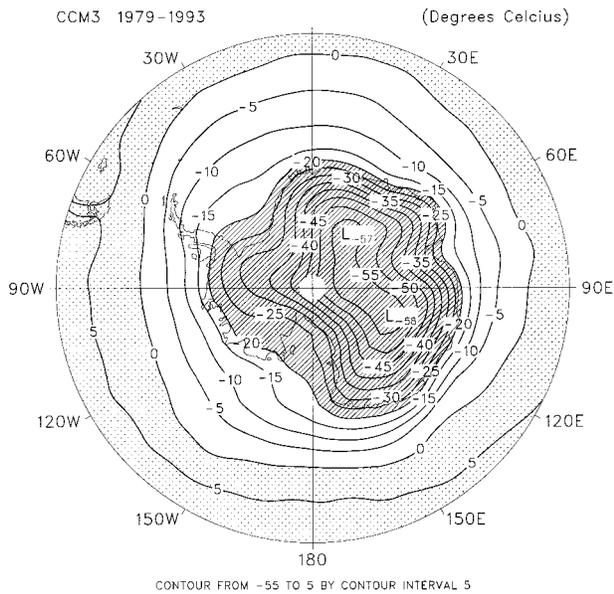
uniform 2-m sea ice of complete horizontal coverage, which would suppress coastal temperatures.

Figures 16a,b shows the mean annual surface air temperatures for CCM3 and the ECMWF analyses (1985–92). The latter agrees very well (over Antarctica) with those of Giovinetto et al. (1990), the most up-to-date estimate based on borehole data from 630 sites and shelter temperatures from 60 meteorological stations (see also Cullather et al. 1997). The comparison shows that while the interior of the Antarctic continent is cold by 3°–5°C, CCM3 is especially cold in coastal East Antarctica. A continental-wide 2°–5°C cold bias extends over the coastal ocean out to near the edge of maximum sea-ice cover near 0°C. Such CCM3 cold surface temperatures are not unexpected, since CCM3 sea ice completely covers the grid square and has fixed 2-m thickness. Such ice thickness is greater than that typically observed in the Antarctic (0.5–1.0 m, Allison 1989; Allison et al. 1993). It is commonly observed (Gloersen et al. 1992) that sea-ice concentration (horizontal fractional coverage) is less than 100%, especially in the Antarctic, where 85%–95% concentrations interior to the ice edge are not uncommon. Low sea-ice concentrations would greatly increase heat flux from ocean to atmosphere, resulting in warmer surface temperatures.

5) PW AND $P - E$

The annual PW for both CCM3 and the ECMWF analyses for 1985–92 were compared (not shown). As in the Arctic, the CCM3 PW is less than the analyses by about 10%–20%. (Note that the analyses are biased 10%–15% high, especially for 55°–65°S, decreasing to

(a)   Annual Mean Surface Air Temperature

CCM3 1979-1993   (Degrees Celcius)

CONTOUR FROM -55 TO 5 BY CONTOUR INTERVAL 5

(b)   Annual Mean Surface Temperature

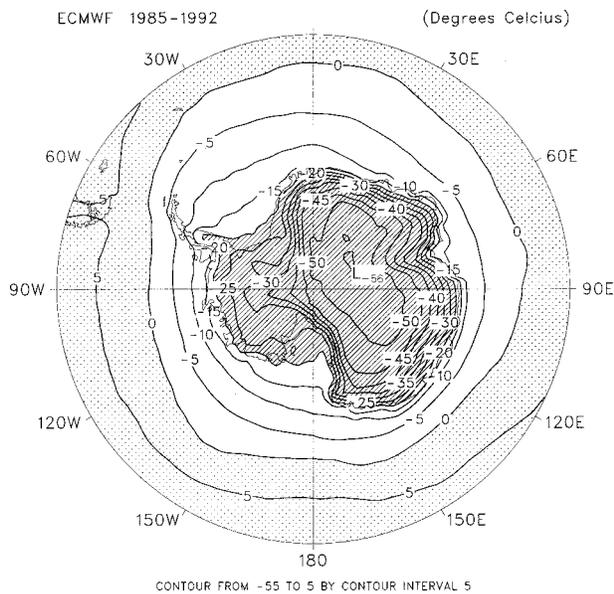ECMWF 1985-1992   (Degrees Celcius)

CONTOUR FROM -55 TO 5 BY CONTOUR INTERVAL 5
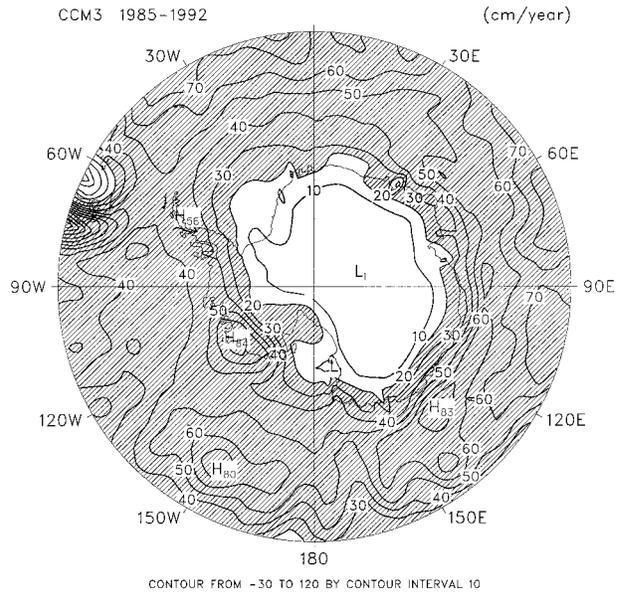
FIG. 16. Ensemble annual mean Antarctic surface temperature (°C): (a) CCM3 AMIP integration (1979–93) and (b) the ECMWF TOGA Archive II for the period 1985–92. Contour interval is 5°C in both (a) and (b). Temperatures greater than 0°C are stippled, and less than −20°C are hatched.

(a)   Annual Precipitation – Evaporation

CCM3 1985-1992   (cm/year)

CONTOUR FROM -30 TO 120 BY CONTOUR INTERVAL 10

(b)   Annual Precipitation – Evaporation

ECMWF 1985-1992   (cm/year)
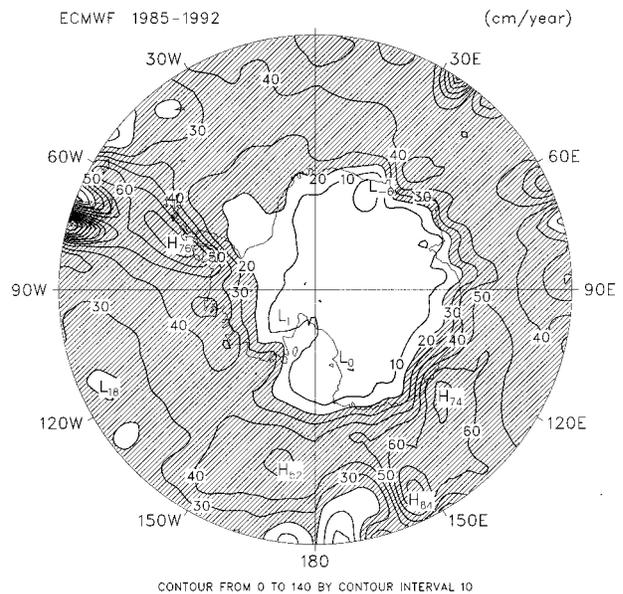

CONTOUR FROM 0 TO 140 BY CONTOUR INTERVAL 10

FIG. 17. Ensemble annual Antarctic ($P − E$ cm yr^{-1}) for (a) CCM3 AMIP integration (1985–92) and (b) for ECMWF TOGA Archive II for the same period. Contour interval 10 cm yr^{-1}, and the region greater than 20 cm yr^{-1} is hatched.

10% at 70°S and much smaller toward the pole; see Bromwich et al. 1995b). The dry East Antarctic plateau is well simulated by CCM3. Overall, the PW patterns of CCM3 are geographically smoother than the analyses around the Antarctic continent. Annual polar cap (70°–90°S) means are 1.7 kg m^{-2} for CCM3 and 2.3 kg m^{-2} for the ECMWF analyses, which is still a significant

difference even accounting for ~5% high bias in the ECMWF value.

Figures 17a,b compare the annual $P − E$ between CCM3 and the ECMWF analyses for Antarctica. Several features of the $P − E$ map are well simulated by CCM3, both in position and in magnitude. The large dry desert of the East Antarctic plateau is well represented. The relative minimum in the western Ross Sea is captured.

The maximum along the coast of West Antarctica in the Pacific sector has the correct position, though somewhat strong in magnitude. However, the maximum along the western coast of the Antarctic Peninsula is only approximately represented, most likely due to topographic smoothing in CCM3. The relative maxima along the East Antarctic coast at 45° and 135°E downstream from the minimum trough centers of Fig. 10a are nicely represented. The band of maximum $P - E$ along 60°S from 150°E to 130°W is present in both CCM3 and the ECMWF analyses. Annual polar cap (70°–90°S) means are 18.1 cm yr^{-1} for CCM3, 14.6 cm yr^{-1} for the ECMWF analyses, and 18.4 ± 3.7 cm yr^{-1} for the observations. The observed value is from Giovinetto et al. (1992) and represents the latest observational estimate with a generous estimate of uncertainty. By most measures, the CCM3 value is well within observational uncertainty.

6) SURFACE ENERGY BUDGET

The CCM3 polar cap (70°–90°S) net surface energy flux (positive into surface) was computed. The region of averaging includes some coastal ocean areas. We note that CCM3 mean annual net surface energy flux around Antarctica ranges from −5 to −20 W m^{-2} near the coast, up to −50 to −70 W m^{-2} for regions just north of the summer sea ice edge. The comparable values quoted in NO88 were based on GCM calculations, and will not be used here. The annual mean net surface energy flux for CCM3 is −5.1 W m^{-2}, with DJF +3 W m^{-2} and JJA −9 W m^{-2}. We note that Briegleb and Bromwich (1998) showed that CCM3 DJF top-of-atmosphere solar absorbed flux was smaller than satellite observations by −22 W m^{-2}, and so we surmise that the CCM3 Antarctic surface energy budget during DJF is low by roughly 20 W m^{-2}.

4. Conclusions

We have presented an assessment of the CCM3 polar climate simulation. We have shown that CCM3 is able to well simulate many important climatic features of both polar regions, and that in general, CCM3 is an improvement over CCM2. We now present a unifying summary of the CCM3 polar simulation and of the possible causes of simulation deficiencies.

As shown in Briegleb and Bromwich (1998), polar cloud fraction is too high and cloud water paths are too great compared to available observations. This results in too little solar absorption and hence in too strong a polar heat sink. This undoubtedly contributes to the deep polar vortices and cold surface temperatures.

Improved ocean–atmosphere heat exchange over sea ice would reduce polar simulation biases. There is one recent CCM3 integration that has bearing on this topic. The slab ocean model (SOM) of CCM3 (Kiehl et al. 1996) is a simple mixed layer ocean–ice thermodynam-

ics model. Sea ice completely covers the grid square, but thickness and snow cover vary prognostically. An equilibrium integration of CCM3/SOM has been completed. Sea-ice thicknesses in the Arctic were about 3 m, while in the Antarctic about 1 m or less, compared to the uniform 2 m of the control. While surface temperatures cooled 3°–4°C in the central Arctic, and warmed 1°–2° around Antarctica, corresponding to ice thickness and snow cover changes, only a marginal improvement (if any) in SLP occurred. Thus, a more realistic ice thickness, as far as an improved ocean to atmosphere heat flux is concerned, has only a small positive impact on the simulation. Allowing for open water in sea-ice regions, especially in the Antarctic, may have a larger impact on the simulation.

A possible cause of polar circulation biases is due to low horizontal resolution. Bromwich et al. (1994) compare CCM1 R15 and T42 Arctic winter season SLP simulations. They show that the distortion of Icelandic and North Atlantic storm tracks, due to the blocking effect of the broadened Greenland topography at R15 spectral trunction (4.5° lat × 7.5° long), is largely corrected at T42 spectral truncation (2.8° lat × 2.8° long). At low resolution, the Antarctic continent effectively blocks the approach of Southern Ocean cyclones, resulting in a circumpolar trough position that is too far north. The T42 CCM3 simulation does show a northern bias in trough position. Williamson et al. (1995) studied the climate sensitivity of CCM2 to varying horizontal resolutions, from low (R15, T21) to medium (T42) to high (T63, T106; 1.7° × 1.7° and 1.1° × 1.1°, respectively). The goal was to determine if a convergent regime exists in which further refinement of resolution does not significantly change the climate simulation. Many climate statistics vary monotonically with increasing resolution, changing significantly from low to medium and less from medium to high, so that in many cases convergence is achieved between T42 and T63. The general conclusion is that T42 at a minimum is needed, but that higher resolution would be better. Present plans (D. Williamson 1997, personal communication) are to employ a fully semi-Lagrangian dynamics in future versions of CCM, allowing for a longer model time step. This would enable the use of T63 for the same computational cost as the present T42 resolution. Thus, the use of higher resolution (T63) future versions of CCM should have a favorable, if incremental, impact on polar climate simulations.

We now consider errors in global circulation that impact the polar simulation. The mean global circulation biases of uncoupled CCM3 are presented by Fig. 18, which shows the difference in mean annual SLP between CCM3 and the ECMWF analyses. Figure 18 discloses that the polar SLP biases previously discussed are part of a system of planetary scale differences. In the Tropics, the mean centers of strong convection of the Hadley circulation have negative SLP biases of 1–3 hPa, whereas the descending branch of the Walker
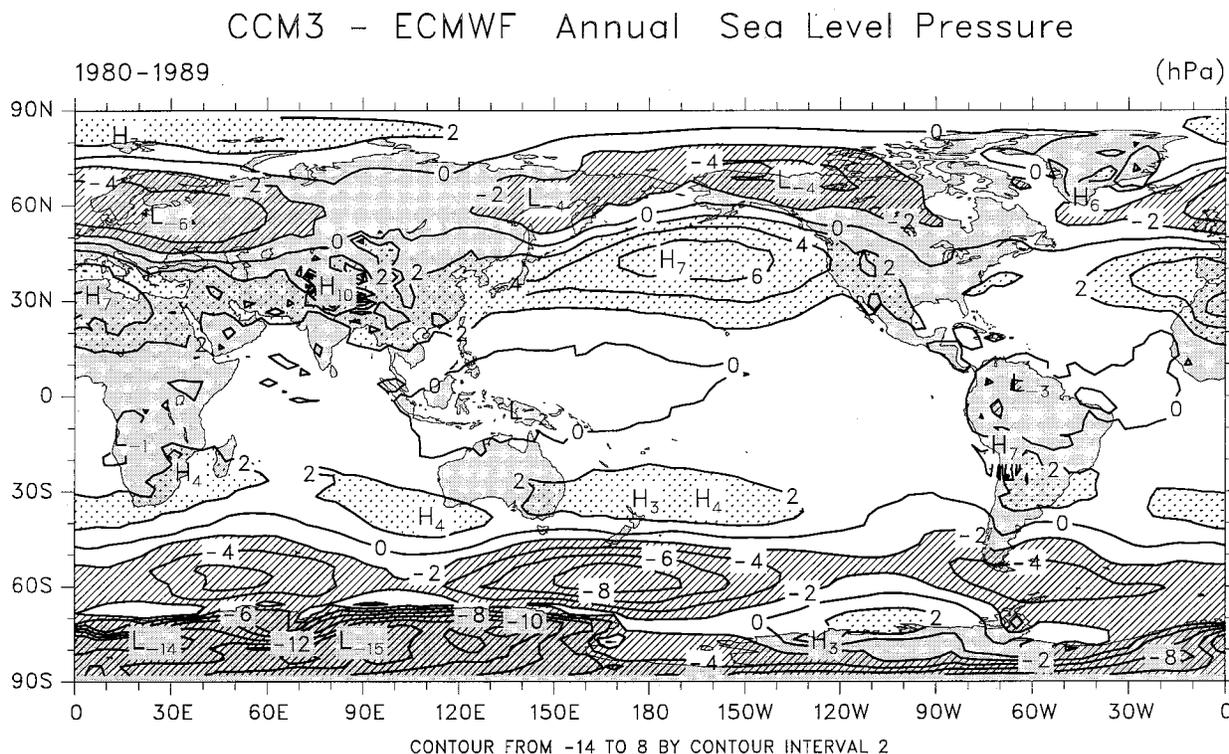
CCM3 – ECMWF Annual Sea Level Pressure

F<small>IG</small>. 18. Mean annual ensemble (1980–89) difference in SLP between CCM3 and ECMWF WMO analyses, with a 2-hPa contour interval. Regions less than −2 hPa are hatched, and those greater than +2 hPa are stippled.

circulation in the eastern tropical Pacific has positive bias (around 1 hPa). Similarly, the descending branches of the Hadley circulation in the subtropics of both hemispheres have positive biases of about 2–6 hPa, while the midlatitude Ferrel cell regimes have zonally varying negative biases from 2 to 8 hPa. Biases in polar SLP patterns have been previously noted. These SLP differences imply stronger trade winds and low-level convergence in the Tropics, stronger midlatitude surface westerlies, and stronger polar easterlies. These SLP and surface circulation biases are similar but somewhat smaller than those of CCM2 at T42 resolution (Hurrell 1995).

These global patterns of SLP bias are suggestive of too strong a global circulation. We have already noted the slightly strong polar heat sinks of the CCM3 simulation. It is possible that there continues to be biases in the tropical heat sources as well. The new deep convective parameterization of CCM3 somewhat improved the tropical precipitation patterns, implying improvement in tropical diabatic latent heating (Hack et al. 1998). The strong ENSO influence on tropical and extratropical variability (Trenberth 1996) is somewhat simulated by CCM3 (Hurrell et al. 1998). The uncertain but potentially significant enhanced cloud shortwave absorption has a strong impact on the global circulation of CCM2 (Kiehl et al. 1995). All of these suggest continuing problems with tropical diabatic heating that cu-

mulatively lead to too strong a global surface circulation. This has implications for coupled CSM integrations.

Indeed, the initial coupled CSM polar simulation shows some of the same biases as noted in this assessment (Weatherly et al. 1998). Other biases, notably in the Arctic sea-ice distribution and the Southern Ocean circulation, probably arise as much from shortcomings in the sea ice dynamics and sea-ice–ocean interactions as they do from atmospheric biases, but the latter do play a significant role.

It is hoped that the improvements suggested here, as well as others being worked on, will result in a next generation CCM with even better polar simulation abilities than that of CCM3. Such CCM developments cannot help but to improve coupled CSM simulations as well.

REFERENCES

Allison, I., 1989: The East Antarctic sea ice zone: Ice characteristics and drift. *Geo. Journal,* **18.1,** 103–115.

——, R. E. Brandt, and S. G. Warren, 1993: East Antarctic sea ice: Albedo, thickness distribution, and snow cover. *J. Geophys. Res.,* **98,** 12 417–12 429.

Battisti, D. S., D. L. Williamson, and R. E. Moritz, 1992: Simulation of the Arctic climatology with the NCAR CCM2. Preprints, *Third Conf. on Polar Meteorology and Oceanography,* Portland, OR, Amer. Meteor. Soc., 130–136.

Bonan, G. B., 1996: A land surface model (LSM version 1.0) for ecological, hydrological, and atmospheric studies: Technical description of user's guide. NCAR/TN-417+STR, 150 pp. [Available from NCAR, Boulder, CO 80307.]

——, 1998: The land surface climatology of the NCAR Land Surface Model (LSM version 1.0) coupled to the NCAR Comunity Climate Model (CCM3). *J. Climate,* **11,** 1307–1326.

Bourke, R. H., and R. P. Garrett, 1987: Sea-ice thickness distribution in the Arctic ocean. *Cold Reg. Sci. Technol.,* **13,** 259–280.

Boville, B. A., and P. R. Gent, 1998: The NCAR Climate System Model, version One. *J. Climate,* **11,** 1115–1130.

Briegleb, B. P., and D. H. Bromwich, 1998: Polar radiation budgets of the NCAR CCM3. *J. Climate,* **11,** 1246–1269.

Bromwich, D. H., and R. I. Cullather, 1998: The atmospheric hydrologic cycle over the Arctic basin from ECMWF re-analyses. *Proc. of the WCRP First Int. Conf. on Reanalyses,* Silver Spring, MD, WCRP, in press. [Available from Int. GEWEX Project Office, Suite 1210, 1100 Wayne Ave., Silver Spring, MD 20910.]

——, R.-Y. Tzeng, and T. R. Parish, 1994: Simulation of the modern Arctic climate by the NCAR CCM1. *J. Climate,* **7,** 1050–1069.

——, B. Chen, and R.-Y. Tzeng, 1995a: Arctic and Antarctic precipitation simulations produced by the NCAR community climate models. *Ann. Glaciol.,* **21,** 117–122.

——, F. M. Robasky, R. I. Cullather, and M. L. van Woert, 1995b: The atmospheric hydrologic cycle over the Southern Ocean and Antarctica from operational numerical analyses. *Mon. Wea. Rev.,* **123,** 3518–3538.

——, Y. Du, and K. M. Hines, 1996: Wintertime surface winds over the Greenland ice sheet. *Mon. Wea. Rev.,* **124,** 1941–1947.

Chen, B., S. R. Smith, and D. H. Bromwich, 1996: Evolution of the tropospheric split jet over the South Pacific Ocean during the 1986–1989 ENSO cycle. *Mon. Wea. Rev.,* **124,** 1711–1731.

Cullather, R. I., D. H. Bromwich, and M. L. van Woert, 1996: Interannual variations in Antarctic precipitation related to El Nino–Southern Oscillation. *J. Geophys. Res.,* **101,** 19 109–19 118.

——, ——, and R. W. Grumbine, 1997: Validations of operational numerical analyses in Antarctic latitudes. *J. Geophys. Res.,* **102,** 13 761–13 784.

Gates, W. L., 1992: AMIP: The Atmospheric Model Intercomparison Project. *Bull. Amer. Meteor. Soc.,* **73,** 1962–1970.

Giovinetto, M. B., N. M. Waters, and C. R. Bentley, 1990: Dependence of Antarctic surface mass balance on temperature, elevation, and distance to open ocean. *J. Geophys. Res.,* **95,** 3517–3531.

——, D. H. Bromwich, and G. Wendler, 1992: Atmospheric net transport of water vapor and latent heat across 70°S. *J. Geophys. Res.,* **97,** 917–930.

Gloersen, P., W. J. Campbell, D. J. Cavalieri, J. C. Comiso, C. L. Parkinson, and H. J. Zwally, 1992: *Arctic and Antarctic Sea Ice, 1978–1987: Satellite Passive-Microwave Observations and Analysis.* NASA, 290 pp.

Hack, J. J., J. T. Kiehl, and J. W. Hurrell, 1998: The hydrologic and thermodynamic structure of the NCAR CCM3. *J. Climate,* **11,** 1179–1206.

Hurrell, J. W., 1995: Comparison of NCAR Community Climate Model (CCM) climates. *Climate Dyn.,* **11,** 25–30.

——, J. J. Hack, B. A. Boville, D. L. Williamson, and J. T. Kiehl, 1998: The dynamical simulation of the NCAR Climate Community Model version 3 (CCM). *J. Climate,* **11,** 1207–1236.

Kahl, J. D., M. C. Serreze, and R. C. Schnell, 1992: Tropospheric low-level temperature inversions in the Canadian Arctic. *Atmos.–Ocean,* **30** (4), 511–529.

Kiehl, J. T., J. J. Hack, and B. P. Briegleb, 1994: The simulated Earth radiation budget of the National Center for Atmospheric Research community climate model CCM2 and comparisons with the Earth Radiation Budget Experiment. *J. Geophys. Res.,* **99,** 20 815–20 827.

——, ——, M. H. Zhang, and R. D. Cess, 1995: Sensitivity of a GCM climate to enhanced shortwave cloud absorption. *J. Climate,* **8,** 2200–2212.

——, ——, G. B. Bonan, B. A. Boville, B. P. Briegleb, D. L. Williamson, and P. J. Rasch, 1996: Description of the NCAR Community Climate Model (CCM3). NCAR/TN-420+STR, 152 pp. [Available from NCAR, Boulder, CO 80307.]

——, ——, ——, ——, D. L. Williamson, and P. J. Rasch, 1998a: The National Center for Atmospheric Research Community Climate Model: CCM3. *J. Climate,* **11,** 1131–1149.

——, ——, and J. W. Hurrell, 1998b: The energy budget of the NCAR Community Climate Model: CCM3. *J. Climate,* **11,** 1151–1178.

Nakamura, N., and A. H. Oort, 1988: Atmospheric heat budgets of the polar regions. *J. Geophys. Res.,* **93,** 9510–9524.

Power, S. B., and L. A. Mysak, 1992: On the interannual variability of Arctic sea-level pressure and sea ice. *Atmos.–Ocean,* **30** (4), 551–577.

Savage, M. L., and C. R. Stearns, 1985: Climate in the vicinity of Ross Island, Antarctica. *Antarctic J. U.S.,* **20** (1), 1–9.

Serreze, M. C., J. D. Kahl, and R. C. Schnell, 1992: Low-level temperature inversions of the Eurasian Arctic and comparisons with Soviet drifting station data. *J. Climate,* **5,** 615–629.

——, R. G. Barry, M. C. Rehder, and J. E. Walsh, 1995: Variability in atmospheric circulation and moisture flux over the Arctic. *Philos. Trans. Roy. Soc. London,* **352A,** 215–225.

Trenberth, K. E., 1992: Global analyses from ECMWF and atlas of 1000 to 10 mb circulation statistics. NCAR/TN-373+STR, 191 pp.

——, 1996: El Nino–Southern Oscillation. *Climate Change: Developing Southern Hemisphere Perspectives,* T. W. Giambelluca and A. Henderson-Sellers, Eds., John Wiley and Sons, 145–173.

——, J. C. Berry, and L. E. Buja, 1993: Vertical interpolation and truncation of model-coordinate data. NCAR/TN-396+STR, 54 pp. [Available from NCAR, Boulder, CO 80307.]

Tzeng, R.-Y., and D. H. Bromwich, 1994: NCAR CCM2 simulations of present-day Arctic climate. Preprints, *Sixth Conf. on Climate Variations,* Nashville, TN, Amer. Meteor. Soc., 197–201.

——, ——, and T. R. Parish, 1993: Present-day Antarctic climatology of the NCAR Community Climate Model Version 1. *J. Climate,* **6,** 205–226.

——, ——, ——, and B. Chen, 1994: NCAR CCM2 simulation of the modern Antarctic climate. *J. Geophys. Res.,* **99,** 23 131–23 148.

Weatherly, J. W., B. P. Briegleb, W. G. Large, and J. A. Maslanik, 1998: Sea ice and polar climate in the NCAR CSM. *J. Climate,* **11,** 1472–1486.

Williamson, D. L., J. T. Kiehl, and J. H. Hack, 1995: Climate sensitivity of the NCAR Community Climate Model (CCM2) to horizontal resolution. *Climate Dyn.,* **11,** 377–397.

——, D. H. Bromwich, and R.-Y. Tzeng, 1996: Further discussion on simulation of the modern Arctic climate by the NCAR CCM1. *J. Climate,* **9,** 1669–1672.